ARCHIVIO ISTITUZIONALE
DELLA RICERCA

Alma Mater Studiorum Università di Bologna
Archivio istituzionale della ricerca

Introducing a base-rocking dual-core braced-frame system equipped with vertical buckling-restrained fuses

This is the final peer-reviewed author's accepted manuscript (postprint) of the following publication:

Published Version:
Ebrahimi Majumerd M.J., Mohammadi Dehcheshmeh E., Broujerdian V., Laghi V., Palermo M. (2023). Introducing a base-rocking dual-core braced-frame system equipped with vertical buckling-restrained fuses. BULLETIN OF EARTHQUAKE ENGINEERING, 2023, 1-23 [10.1007/s10518-023-01776-x].

Availability:
This version is available at: https://hdl.handle.net/11585/943734 since: 2024-03-20

Published:

DOI: http://doi.org/10.1007/s10518-023-01776-x

Terms of use:

Some rights reserved. The terms and conditions for the reuse of this version of the manuscript are specified in the publishing policy. For all terms of use and more information see the publisher's website.

This item was downloaded from IRIS Università di Bologna (https://cris.unibo.it/).
When citing, please refer to the published version.

(Article begins on next page)

10 November 2026

This is the final peer-reviewed accepted manuscript of:

Ebrahimi Majumerd, M.J., Mohammadi Dehcheshmeh, E., Broujerdian, V. et al.

Introducing a base-rocking dual-core braced-frame system equipped with vertical buckling-restrained fuses.

In: Bulletin of Earthquake Engineering 21, 6453–6476 (2023)

The final published version is available online at:

https://doi.org/10.1016/j.jcsr.2019.105858

Rights / License:

The terms and conditions for the reuse of this version of the manuscript are specified in the publishing policy. For all terms of use and more information see the publisher's website.

This item was downloaded from IRIS Università di Bologna (https://cris.unibo.it/)

When citing, please refer to the published version.

Introducing a base-rocking dual-core braced-frame system equipped with vertical buckling-restrained fuses

Mohammad Javad Ebrahimi Majumerd[a], Esmaeil Mohammadi Dehcheshmeh[a], Vahid Broujerdian[a], Vittoria Laghi[b], Michele Palermo[b]

[a] School of Civil Engineering, Iran University of Science and Technology, Tehran, Iran.

[b] Department of Civil, Chemical Environmental and Material Engineering, University of Bologna, Bologna, Italy.

Abstract

A base-rocking dual-core braced-frame (BRDC) system equipped with vertical buckling-restrained fuses (BRF) is developed to prevent the soft-story failure mechanism. The proposed system comprises two elastic cores connected by BRF between the floor levels. BRFs are used as replaceable fuses in this system to dissipate the input energy and reduce the seismic responses. The seismic performance of the proposed system is evaluated using a new time history analysis method called endurance time (ET). The method is numerically applied in three structures with different heights, specifically 12, 15, and 18 stories. The truncated design spectra method is used to design the cores. The results show that the proposed system resolves both the problem of column uplifting and the large cross-section needed for post-tensioned cables in the rocking systems.

Keywords: Non-linear Analysis; ET Method; Interchangeable Fuse; Rocking Dual-Core; Seismic Evaluation.

1 Introduction

Compared to the fixed-base conditions, the rocking mechanism of structures at foundation is known as a way to reduce the seismic base-shear resulting in lower ductility demands [1]-[2]. Besides, previous studies show that the conventional energy dissipation that occurs in the gap opening at the base can be converted to an equivalent viscous damping ratio of 2 -6% for most typical structural configurations [3]–[5]. Vertical accelerations and forces due to vertical modes excited by the seismic impact have also been studied [6]-[7], and in some examples of rocking steel bridge piers, it approximately doubles the vertical forces [6]. Lu [8] identified a restoring force when an uplifting wall or rocking edge is attached to the surrounding floor and has an upward motion.

Braced frame systems absorb the seismic energy through large plastic deformations, causing the accumulation of lateral deformations into a single story due to the relative strength and stiffness distributions along the building height. Therefore, medium and high-rise braced frame systems are prone to soft/weak story failure mechanisms [9]. In addition to the soft/weak story mechanism, repairing and replacing the damaged members after an earthquake might be economically unfeasible [10]. Furthermore, braced frame systems suffer from low ductility and low energy absorption caused by the buckling of the braces under compression before yielding. Given that the loading capacity of the brace decreases after buckling, its hysteretic curve becomes asymmetric, and the Energy Dissipation (ED) is reduced [11],[12].

Nowadays, modern rocking systems are developed to prevent the creation of soft-story mechanism, which are repairable and have higher ductility [9],[13]. Nonetheless, their use is limited due to column uplifting issue and the need for large post-tensioned cables in medium to high-rise buildings [14]-[16]. In recent years, three types of rocking systems with column uplift mechanisms have been reported, including: (1) Midorikawa rocking system [17], (2) Tremblay

controlled braced Steel frame [18], and (3) Pollino and Bruneau rocking core [6] (**Fig. 1**). In the first system (**Fig. 1a**) the base plates under columns have the capability of yielding and dissipating energy. By comparing this system with a conventional frame, the maximum base shear of the frame with the yielding base plate is significantly less than the latter. The second system (**Fig. 1b**) adopts viscous dampers to dissipate seismic energy. In this system, the frame with a rocking function can withstand seismic action without suffering structural damage or exceeding code-specified limitations. The third system (**Fig. 1c**) used buckling restrained braces (BRBs) as ED fuses at the base. In this case, the structure is restored to its original position through the bending moment associated with its self-weight.

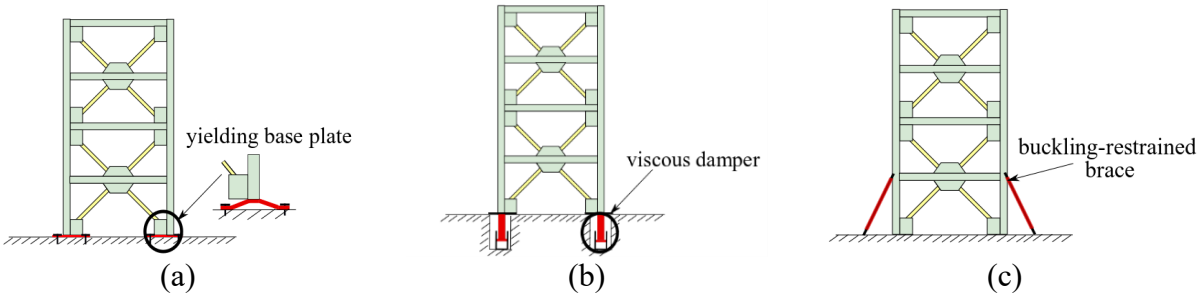

Fig. 1. The rocking systems proposed to prevent soft-story response; (a) Midorikawa rocking system [17] (b) Tremblay controlled braced Steel frame [18]; (c) Pollino and Bruneau rocking core [6].

In all the above-mentioned systems, the rocking movement causes the uplifting of columns from the foundation. Column uplifting, in turn, intensifies the lateral displacements in higher structure modes, consequently increasing the design forces [15].

The concept of the strongback was developed to prevent the column uplifting [15] which increases the ductility using buckling restrained braces without changing the stiffness [16]. Different strongback systems have been proposed so far including: (1) Lai and Mahin spine frame [19], (2) Shuling strongback [20], (3) Takeuchi spine truss frame [14], (4) Liang tied eccentrically braced frames [9], (5) Palermo et al. dual system [21] (**Fig. 2**). In the first system (**Fig. 2a**), the structure consists of an elastic core that is pinned to the ground and a BRB to dissipate energy. Considering

66 the use of the elastic core, the results of time history analyses showed a relatively uniform drift in
67 these structures [19]. Similar configurations were studied by connecting a conventional frame
68 structure with a strongback system [22]–[25]. The second system (**Fig. 2b**) includes a rocking core
69 and a tension-only brace cable used as brace and ED. The time history analysis results showed that
70 inter-story and roof drifts are within allowable ranges [20]. In the third system (**Fig. 2c**), the
71 buckling-restrained columns are located at the base floor of the rocking core to absorb large
72 deformations and prevent damages caused by buckling of the first-floor column. This system
73 reduces the inter-story drifts and also the forces acting at the foundation [14]. In the fourth system
74 (**Fig. 2d**), the structure consists of two cores connected by ductile links on adjacent floors. Similar
75 to the previous systems, this one keeps the structure in the first mode during an earthquake
76 excitation, thus preventing the occurrence of a soft-story failure mode [9]. In this system, the steel
77 shear links increase the stiffness, energy absorption and also the resistant moment arm [26]. In the
78 fifth system (**Fig. 2e**), the strongback configuration is combined with a moment-resisting frame to
79 enhance the seismic performance and a fluid-viscous dampers to dissipate the seismic energy [26].
80 An important issue when using strongback systems in high-rise buildings is the increased shear
81 forces and bending moments caused by higher-modes effect. To resolve this issue, multiple
82 rocking segment systems are developed [27]. Recently, a new design method has been proposed
83 for innovative types of self-centering rocking dual-core systems [28], [29]. In existing rocking core
84 design methods, both force-based and displacement-based methods are required to estimate the
85 peak seismic displacement [18]–[20].

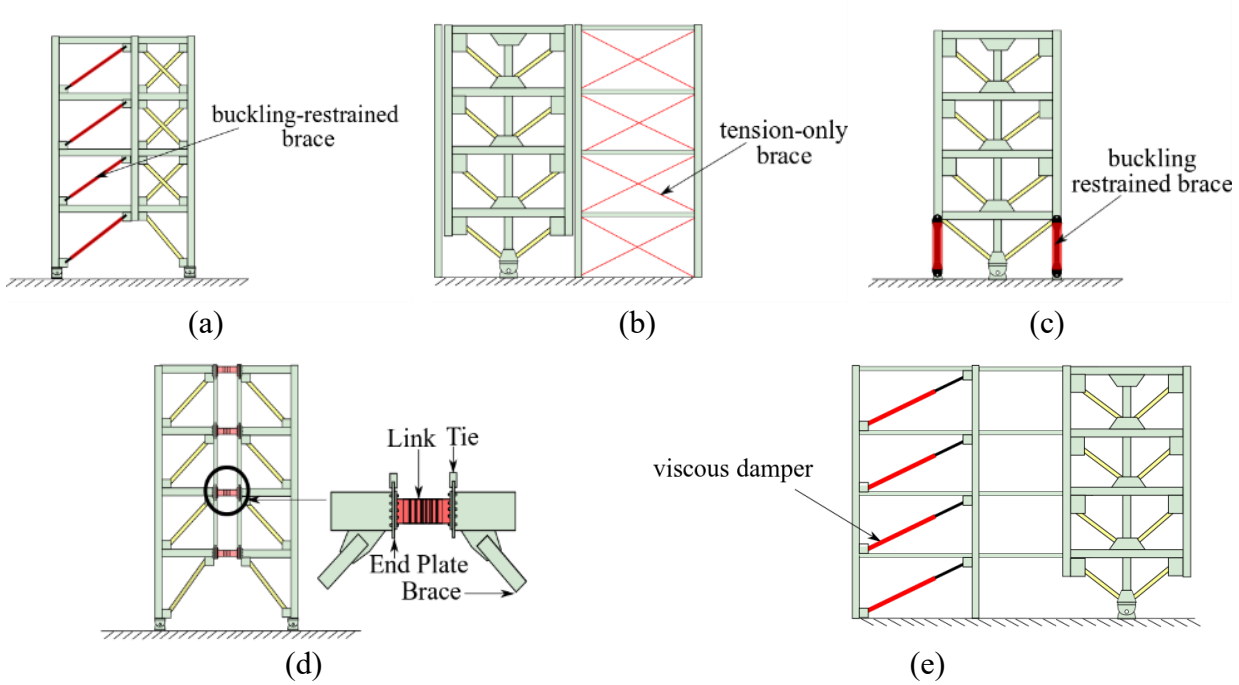

Fig. 2. The available strongback systems to prevent soft-story failure mode; (a) Lai and Mahin spine frame [19]; (b) Shuling strongback [20]; (c) Takeuchi spine truss frame [14]; (d) Liang tied eccentrically braced frames [9]; (e) Palermo et al. dual system strongback [21]

This study proposes a base-rocking dual-core braced frame equipped with vertical buckling-restrained fuses (BRDC-BRFs). The fuses placed between the two elastic cores increase the energy dissipation and reduce the structural response. The main feature of the BRDC-BRF system is twofold: (i) to prevent the creation of a soft-story failure mechanism and (ii) to facilitate the replacement of EDs after seismic hazards. This study aims to introduce the BRDC-BRF system as an effective earthquake-resistant solution to mitigate the seismic effects on high-rise buildings. Moreover, a new design method is proposed for BRFs and core elements with reduced computational effort. For this purpose, the system is validated through non-linear time-history analyses on structures with 12, 15, and 18 stories using Endurance Time (ET) method. The ET method is a new performance-based method for seismic analysis and design of structures. In this method, the structure is subjected to special ground motions with increasing intensity. The time needed for the damage index (such as the inter-story drift) to reach a certain level of performance

or failure is defined as the structure's endurance time (ET). Thus, a structure with a higher ET would have a better performance against earthquakes. ATC 58 approach [30] to seismic loss assessment uses IDA needing a lot of time-consuming analyses. However, the ET method is part of the demand-driven predicting process and is a computationally more efficient alternative to IDA [31]. Generally speaking, the main advantages of the ET method relative to the prevailing Incremental Dynamic Analysis method (IDA) are the following: (i) less computational effort for seismic assessment, (ii) applicability to a variety of structures and behavioral complexities, and (iii) applicability in laboratory works [32]. Ref. [33] estimated the ET method's target time for different seismic risk levels. In this study, each seismic risk level considered a specified time of Endurance Time Acceleration Functions (ETAFs). For instance, the 10 and 15 seconds time are considered for DBE and MCE levels, respectively.

2 Materials and methods

2.1 System description

The proposed BRDC-BRF system is schematically shown in **Fig. 3**. The system consists of two cores composed of beams, braces, ties, and columns. The arrangement of the structural members is similar to that of an EBF system. As shown in **Fig. 3b**, the applied lateral loads cause rotation at the base of the columns around the system's cores. BRFs are placed vertically in the system to increase the system performance under seismic action, as demonstrated in Appendix 1. Regarding the elastic deformation of the system, this rotation can be considered a rigid core rotation. The rotation of the BRDC-BRF causes the BRFs to act either in tension or compression. The BRFs between the cores increase the stiffness, dissipating energy and reducing the structural response. The BRDC-BRF system has to be appropriately connected (as detailed in section 2.5) to the floor diaphragm by adjacent columns, thus constraining the lateral displacements of the system and preventing global instability of the whole structure. The relative vertical displacement between

two cores of BRDC-BRF is large under lateral load, while the rest of the diaphragm displacements are horizontal. For this reason, this part of BRDC-BRF should not have any vertical connection to the diaphragm. Of course, diaphragms and connecting/support beams play a vital role in the global stability of the system. If they are not properly designed, the global stability of the system may be compromised under lateral load and even gravity loads. Section 2.5 presents a possible detail to connect the core to the diaphragm.

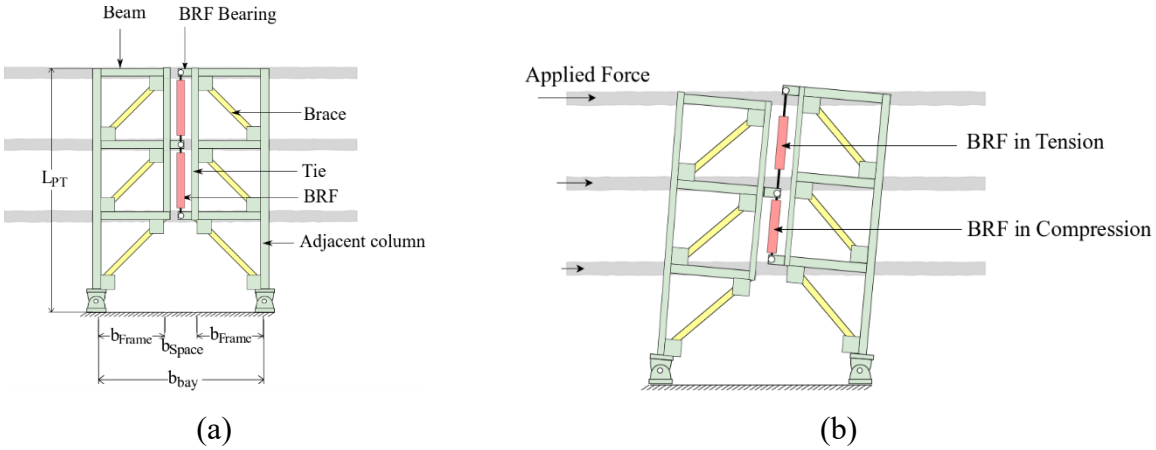

Fig. 3. Schematic of BRDC-BRF system: (a) initial position; (b) "rocked" position

2.2 Research method

The research method adopted in the present work is shown in the flowchart of **Fig. 4**. The core design is based on a preliminary design of BRFs to set an initial value of the cross-sectional areas. Then, the core is designed and verified through a step-wise procedure based on the development of dynamic time history analysis (here implemented with the finite element software SAP 2000). The design steps are as follows:

1. An initial value for the BRF area is assumed based on a preliminary design.
2. The lateral forces for structural balance are determined by applying the BRFs yield force to determine the first loading stage. In this case, the lateral load is assumed to be triangular.
3. The core and BRFs (with post-yielding stiffness) are simulated by a finite element software.

4. The loads obtained from the first loading stage, gravity loads, and the forces corresponding to the axial capacity of BRFs, are applied to the structure. Then, the truncated spectrum is introduced into the software to estimate the effects of higher modes (second stage of loading) in the structure [28] and [34].
5. After analyzing the structure with the pre-determined forces, the structure design process is completed. If needed, the cross-sections obtained in Step 1 are updated accordingly.
6. The structure is then analyzed under the design basis earthquake (DBE) and maximum considered earthquake (MCE) level records using the time history method.
7. The capacity of all members is evaluated under seismic load. Thus, the maximum strains examined for all sections are compared with the acceptable limit (the member's yield strain). If the strain exceeds the allowable limit, the design is repeated with an increased load coefficient in the second stage.
8. The values of peak roof drift are checked, and if they are not suitable, the cross-sectional area of the BRFs is increased. This step requires checking the roof drift to determine BRFs and cores stiffness (see section 3.2.2).
9. The maximum values of the inter-story drift are checked, and if they are not suitable, the load coefficient of the second stage is increased. In this step, checking the inter-story drift is necessary to determine the story member stiffness of the core (see section 3.2.2).
10. In the final step, the structure is verified considering current seismic code provisions (thus including all necessary seismic intensity levels based on the specific building typology).

It must be noted that during the system design, no local or global buckling is accounted to prevent a soft-story mechanism. Global and local buckling of the structural members (outside of the strongback system) should be checked separately.

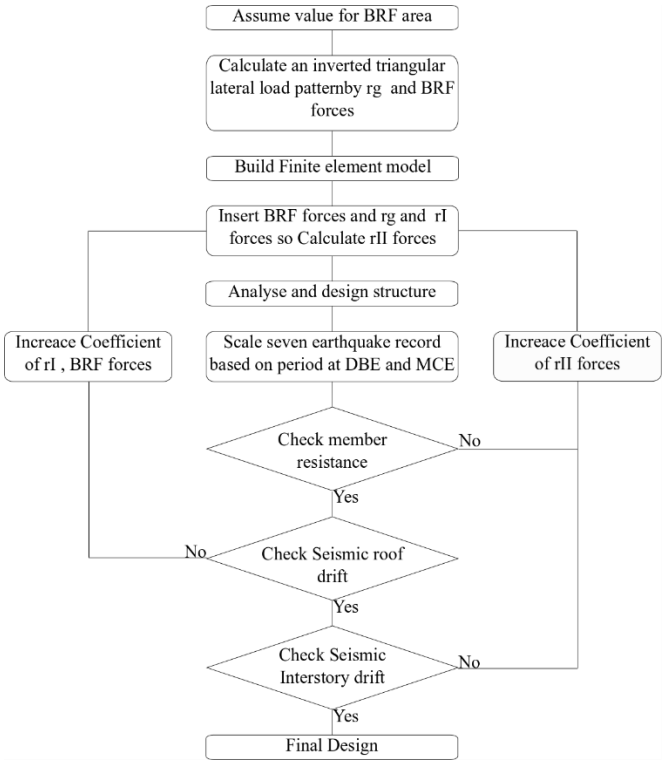

Fig. 4. Design flowchart for BRDC-BRF: a) preliminary design with the simplified model; b) detailed design with finite element model

2.3 Design criteria

As mentioned earlier, after considering the BRF cross-sectional area, the following section deals with the core design in terms of the effects of the first and higher modes and checks for the design assumptions. The design process of the core is such that the core would be under two sets of loads. The first set of actions created in the core is related to the effect of the first mode, which according to the capacity of the designed members, ED is achieved. The second set of actions generated in the core is related to the effect of higher modes, the values of which are calculated using the truncated spectrum.

In the second part of the design process, the cross-sections of rocking cores under lateral forces caused by the first and higher modes are determined. Compared to conventional braced frames, the main feature of the BRDC-BRF system is the capacity created by the cores to yield

simultaneously in all BRFs at all stories. Therefore, the deformation profiles and BRDC-BRF vibration modes in the inelastic range can be easily predicted. This is not true for conventional bracing frames, which can display complex, variable, and unpredictable profiles during seismic excitation [34].

Since the core deforms laterally during reciprocating motions, the lateral response caused by higher modes would be increased by the flexibility of the core and the presence of the horizontal floor diaphragm at the core height. The dynamic response is mainly controlled by the flexural and shear stiffness of the core, as the stiffness of BRFs would slightly decrease with yield.

This assumption is the basis of the analytical method presented in this section for predicting design forces created by higher modes in core members. This method includes a modal superposition method in which the share of individual modes in each response rate, such as the forces of the core members to obtain the overall response or the demand for force $\boldsymbol{r}$, is summarized as follows [34]:

$$r(t) = \sum_{n=1}^{N} r_n(t) \tag{1}$$

The modal superposition creates an accurate solution using the modal properties of the structure and a sufficient number of modes. Equation (1) applies to both elastic and inelastic systems. For BRDC-BRF, inelastic modal properties can be obtained by assigning reduced stiffness to BRFs. The reduced stiffness of BRFs is considered equal to their secondary stiffness.

Therefore, the analysis method combines the force demand from the yield of BRFs in the first mode with the additional forces created by the dynamic response in the second and higher inelastic modes. For the design BRDC-BRF system, two forces are considered include $\boldsymbol{r_I}$ (set I) and $\boldsymbol{r_{II}}$ (set II). For design purposes, only a conservative estimation of the maximum expected value of $r(t)$ is required, and a simple absolute value combination can be used to achieve design values [34]:

$$|r(t)|_{max} = |r_I(t)|_{max} + |r_{II}(t)|_{max} \quad (2)$$

Set I (r_I) can be obtained from the static analysis when all BRFs have reached their expected strength [28], [34]. The forces of set II (r_{II}) are obtained from the analysis of the modal response spectrum performed with a numerical model whose BRFs stiffness is reduced [28], [34].

2.4 Numerical model

Non-linear static and dynamic numerical simulations were performed using OpenSees [35]. These models include support columns to calculate the stiffness of a gravity loads system, such as mass and diaphragm force.

As shown in **Fig. 5**, the main members of the numerical model are the buckling-restrained columns and the BRDC-BRF core members (beams, braces, columns, and ties). The BRF members are modeled as corotTruss with Steel02 uniaxial material [36], and core members are modeled as forceBeamColumn with elastic uniaxial material. To consider the gravity loads of middle frames and P-delta effects, lean-on column is modeled according to references [37]–[39].

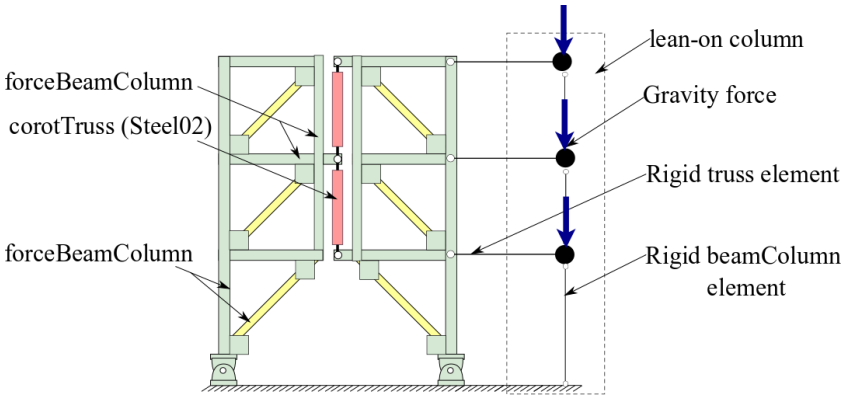

Fig. 5. The 3-Story BRDC-BRF with lean-on column

2.4.1 Prototype structure properties

The analysis is performed on three structures of 12, 15, and 18 stories, located on type C soil for the Los Angeles area following ASCE7 [40]. In all systems, the height of the first floor is 4.572

meters, and the height of the other floors is 3.66 meters. The span length is 6 meters, and the openings with rocking cores are considered to be 0.5 meters longer due to the location of the BRFs between the cores. As it is shown in **Fig. 6a**, rocking cores are used along each of the four axes, and on each axis, three cores are used.

Some basic assumptions were made to estimate gravity load and seismic mass. Dead loads, including concrete floor slab, steel floor deck, mechanical equipment, floor and ceiling finishes, and the approximate weight of each square meter of the structural skeleton, are estimated. The distributed dead loads used for the design are 4.20 kPa, 4.16 kPa, and 2.45 kPa for the first, middle, and roof floors, respectively. The seismic masses for each self-centering frame are 1256, 1250, and 627 tons for the first, middle, and roof floors, respectively. The live load distributed in the first and middle floors, the roof load, and the partition load were 2.39 kPa, 0.96 kPa, and 0.72 kPa, respectively [15]. In time history analysis of BRDC-BRF structures, Rayleigh damping of 5% is considered. It must be noted that the verification of the numerical modeling has been performed based on the available experimental data [41], and the results are reported in [28].

2.4.2 Ground Motion Datasets

According to the rules of the ASCE41 code [42], at least three series of ground motions should be used for structural purposes for the time history analyses. These ground motions should be selected in such a way that they are as similar as possible in terms of geological, tectonic, seismic, and especially soil layer characteristics. If seven series or more ground motions are used, the average values of the structural response can be used. Otherwise, the maximum response of the structure must be considered [42].

In the current research, seven ground motions were selected from a set of 20 records of FEMA440 code [43]. The soil of these ground motions was type C (S_1=1.5 and S_s=0.6) according to ASCE7

[40]. In the first step, seven ground motions, known as the GM set, were scaled regardless of the hazard level so that the level below the quasi-acceleration spectrum equals the level below the 2800 code spectrum. The interval period for this scale was set from 2 to 5 seconds. The purpose of this scaling was due to the sensitivity of the non-linear analysis to the intensity and magnitude of the earthquake; thus, it was considered best to keep the range of each ground motion as close as possible to the range of regulations. **Table 1** shows the characteristics of the ground motions of the GM set, and the scale coefficients used, hereinafter referred to as the Estekanchi coefficients [44].

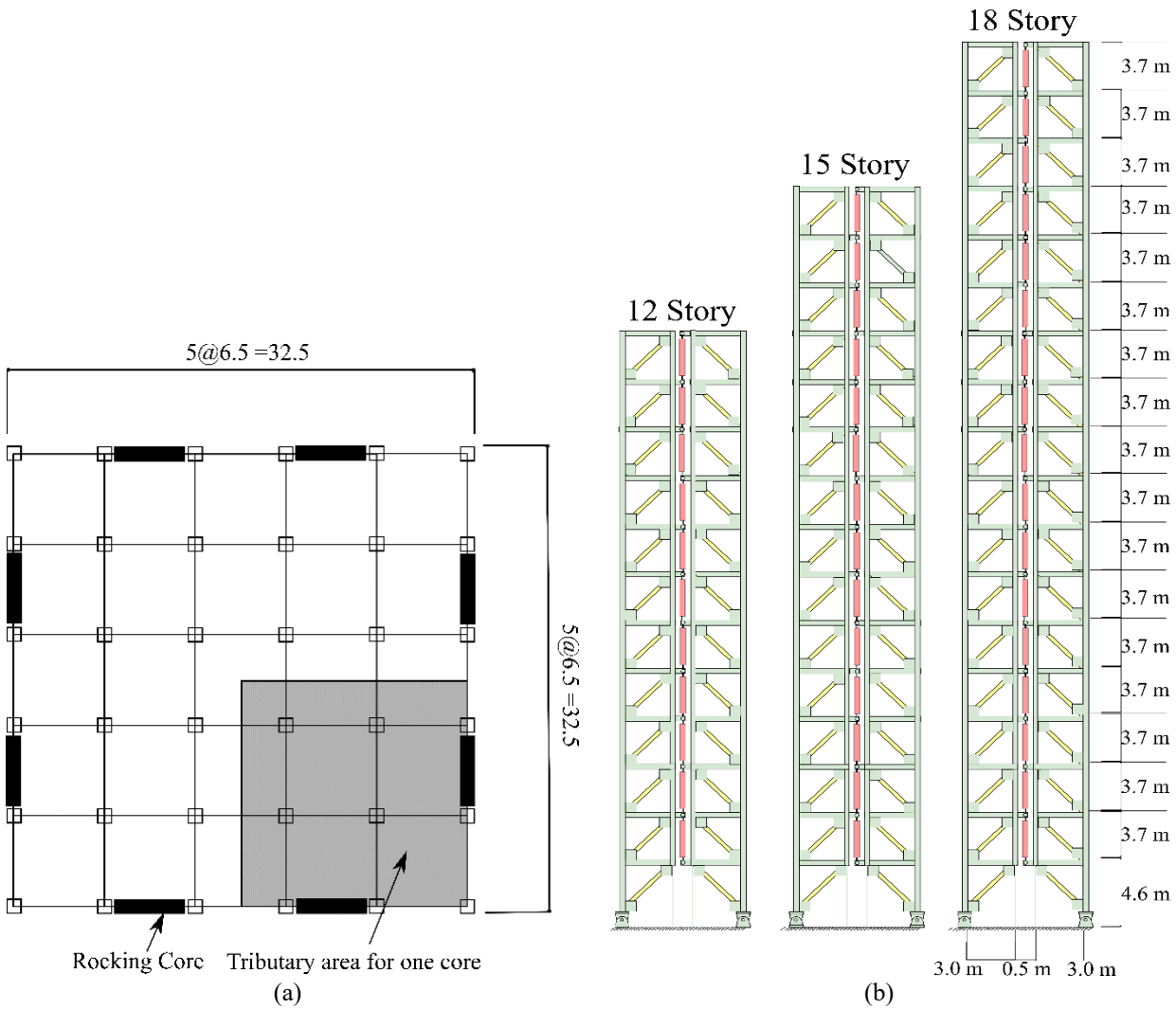

Fig. 6. Prototype building used for the parametric study: (a) typical floor plan; (b) elevation

In the next step, these GM set are scaled by considering the hazard level so that the level below the average of their pseudo-acceleration spectrum was equal to the level below the spectrum of ASCE41 code in two risk levels BSE-1 (DBE) and BSE-2 (MCE). The interval period for this scale was set from 0.2 to 1.5 seconds. This coefficient of scale would eventually be multiplied by the Estekanchi coefficient. If the conservative method suggested by the code is used to scale the ground motions, it may cause a significant difference between the mean and code spectrum [44].

Table 1. Summary of 7 ground motion characteristics

Station ID No.	Earthquake Name	Component	Year	Station Name	EpiD (km)	Scale Factor
57383	Morgan Hill	90	1984	Gilroy Array #6	36.34	1.8360
1652	Loma Prieta	250	1989	Anderson Dam (Downstream)	26.57	2.6092
47006	Loma Prieta	67	1989	Gilroy - Gavilan Coll.	28.98	2.2040
58065	Loma Prieta	0	1989	Saratoga - Aloha Ave	27.23	1.437
58135	Loma Prieta	360	1989	UCSC Lick Observatory	16.34	2.289
12149	Landers	0	1992	Desert Hot Springs	27.33	3.6378
24278	Northridge-01	360	1994	Castaic - Old Ridge Route	40.68	1.073

2.4.3 Endurance Time (ET) Method

The concept of the Endurance Time Method can be well explained with a hypothetical test. For example, the structural performance of three different structures (3-, 6-, 9-story) with uncertain characteristics against earthquakes are investigated. In order to check the performance of these structures, they are placed on a shaking table. The test begins with the excitation of the shaking table, which gradually increases in intensity over time (acceleration function). Likewise, the drift range of the three structures is also gradually increasing. Due to the increasing demand for the acceleration function of the structures, they reach the yielding state and the stage of non-linear behavior from the elastic deformation and finally get the overall dynamic instability. During the test, the values of response quantities or damage index can be plotted directly in terms of time. For

example, the maximum ratio of the roof drift as damage index is plotted in **Fig. 7**. As can be seen, the range of damage index in frame 9-story is less than the others. So, it can be said that the performance of this system is more than the other two structures in different intensities.

As a result, according to this time and the corresponding intensity of the structure's excitation, increasing the endurance time can result in high performance at the specified damage limits. In addition, if the acceleration function is calibrated to meet the code's design requirements, a minimum acceptable endurance time for the practical design phase is met. The increasing trend of the acceleration function gives a special meaning to the time parameter in the endurance time analysis. It can be said that time represents the measure of intensity.

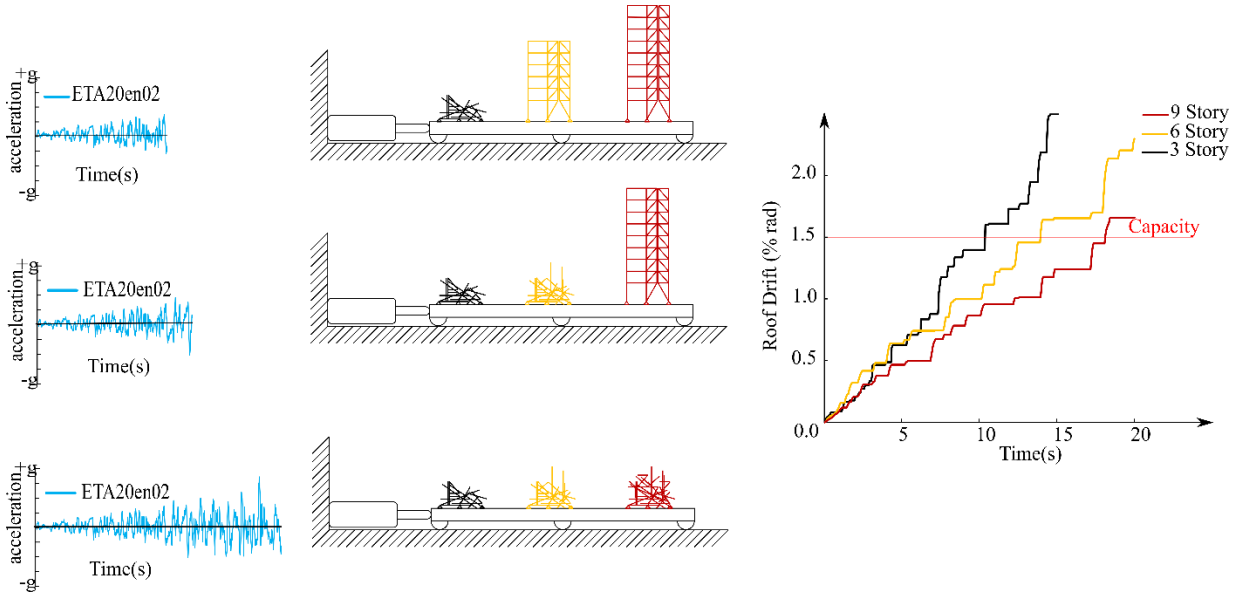

Fig. 7. Basic concept of ET analysis

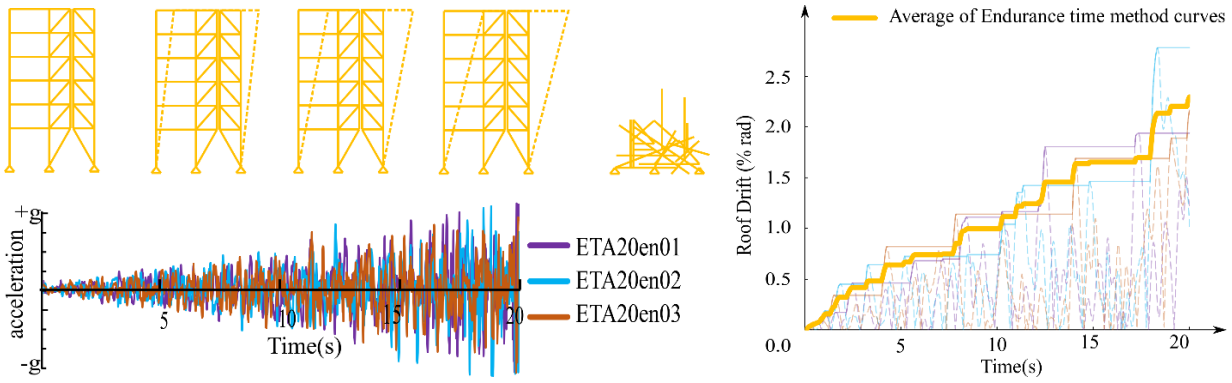

285 **Fig. 8.** Calculate endurance time curve analysis; (a) endurance time method functions; (b) endurance time curves.

286

287 As an illustrative example, **Fig. 8** shows how to plot incremental diagrams of the ET method for a
288 6-story structure. The peak roof drift is considered a damage index in this figure. The obtained
289 smoothed curve can be considered as the structural performance curve. In this method to extract
290 the structural performance curves, after performing the analysis, the desired response quantities
291 (such as maximum roof drift) are obtained over time, and the maximum absolute response value
292 at each time is determined. After smoothing the obtained diagram using the moving averaging
293 method, the final/mean-smoothed curve is plotted (**Fig. 8b**). In this diagram, the value of response
294 quantity or damage index at any time indicates the earthquake demand with a return period equal
295 to each ET of the structure [45].

296 The ETAF series corresponding to the average of real earthquakes [41], named en01-03 (ETA20),
297 were constructed to estimate the non-linear response of real earthquakes. So that the spectrum of
298 this series in the tenth second corresponds to the average pseudo-acceleration spectrum of the GM
299 set after applying the initial scale coefficients. The capability of ETAFs in predicting the behavior
300 of structures under selected Ground Motions has been proven in previous studies by Estekanchi et
301 al. [46]. Therefore, a good estimate of the structure behavior can be obtained by correct scaling
302 and selecting the appropriate time to apply the series of ETAFs.

303 The series of ETAFs, optimized for the pseudo-acceleration spectrum average of 7 GM series in
304 the elastic range (R=1), is also optimized for drift spectrum in the elastic and non-elastic range (R
305 = 1, 2, 4, and 8). These functions are expected to better adapt the structure evaluation in the
306 inelastic range. The acceleration function is optimized for 71 points between periods of 2 to 5
307 seconds and 10 points between periods of 20 to 50 seconds. This method uses 0 to 10 and 15
308 seconds of ET time series for the DBE and MCE levels, respectively.
309

310 **2.5 Connecting core to diaphragm details**

311 The floor diaphragms and connecting/support beams between two cores are essential in this
312 system's lateral stability. The cores and diaphragm's connection and isolation must be made with
313 particular attention in the proposed system. The connection of these two is to provide stability and
314 transfer lateral loads. The isolation avoids the diaphragm's failure and the increasing system's
315 lateral stiffness.

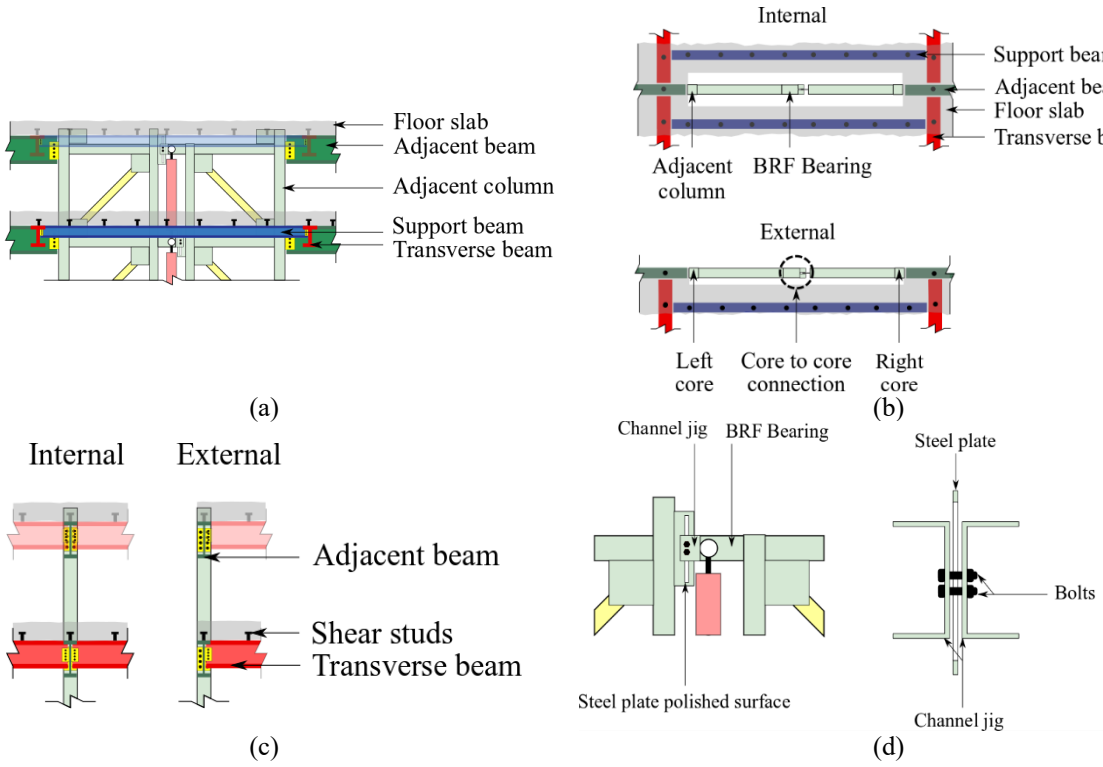

316 **Fig. 9.** Detailing of the isolated core to the diaphragm; (a) front view; (c) plan view of the internal and external core;
317 (c) section, internal and external core; (d) front view of core-to-core connection.
318
319 Therefore, the design of the core-to-diaphragm connection system is a critical aspect and must be
320 conducted with the required care as detailed here. A specific connection system is proposed to
321 isolate the rocking cores to the floors and transmit the lateral load of the diaphragm to the cores.
322 The idea is that the core and the diaphragm should not interfere with each other's proper
323 performance. Moreover, the diaphragm should be able to transfer lateral load effectively and
324 should not be damaged due to the rotation of the core. Also, the core should be able to rotate. In
325 **Fig. 9a** and **9b**, the diaphragms are connected to the adjacent columns of the core. The adjacent
326 beams transmitted seismic diaphragm loads to the core. The rocking cores can be used in the
327 internal or external part of the plan (**Fig. 9b** and **9c**). The transversal and support beams provide
328 the integrity of the diaphragm in the perimeter of rocking cores (**Fig. 9**). According to this figure,
329 the dual cores are located in the diaphragm; they will not come close to each other when subjected
330 to lateral load; this is because the dual cores' adjacent columns (the core side columns) are
331 connected to the diaphragm using pinned connections. Therefore, lateral instability is not observed
332 in this system. In this figure, the beam-to-beam and beam-to-core connections are pinned types.
333 The dual cores at the junction must be constrained to move out to the plane. For this purpose, the
334 details of **Fig. 9d** are provided to connect them at the level of the diaphragms. In these figures, the
335 rotation of the dual cores relative to each other is easily done. Also, the cores are not connected to
336 the diaphragm in this area. This core connection is connected with the diaphragms to prevent global
337 instability of the core. It should be noted that the lateral connection of the core-to-diaphragm
338 should not have much effect on the performance of the two members.
339

3 Results and Discussions

3.1 Design of the elastic core

This section determines the core's rocking sections under the loads described in Section 2.3.2. By determining the load Set I, the initial design caused by the forces of the first mode of the structure can be assessed, and the cross sections of the structural members can be determined. After the initial design, the intended states of the BRFs stiffness effect have been investigated to determine the load Set II. **Fig. 10** shows the four modes of vibrations obtained from the numerical simulations considering the elastic and inelastic axial stiffness of the BRFs. In the first case, the stiffness of BRFs is considered elastic, and in other cases, the stiffness of BRFs is considered their secondary stiffness.

As **Fig. 10** shows, the shapes of the frame modes with the element stiffness are almost identical in the elastic and inelastic states. The periods of the frames are affected by the BRFs stiffness; Still, this effect is more significant for the first mode and gradually decreases for higher modes until the deformation of the elastic core contributes more to the modal shape. The inelastic state in the first mode, with a definite deformation pattern and uniform yielding of BRFs' member forces, can be obtained from simple static analysis. In the proposed analysis method to determine the forces of Set II, multimodal response analysis should only be considered in the case of inelastic analysis of higher modes because the response in these modes generates additional inertial loads in the core elements. The modal properties of the elastic system were also used for comparison. As shown, the difference between the elastic and inelastic states and the associated period is slight for higher modes. Thus, the effect of reduced stiffness is limited, and the analysis will not be sensitive to the reduction in stiffness values assigned to the BRFs to create inelastic modal properties.

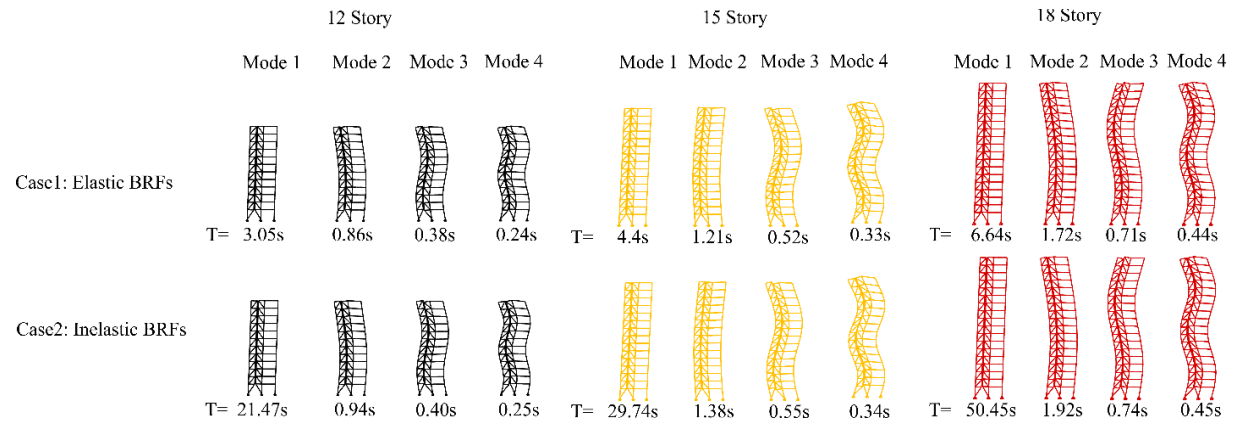

Fig. 10. Vibration modes of 12-, 15-, and 18-story numerical models

Response spectrum analysis in SAP2000 software [42] has been used to determine the load Set II. The effect of the first mode is removed from the response spectrum curve introduced to the software. For this reason, the response spectrum can be considered zero for larger or equal periods to the first mode period. **Fig. 11** shows the truncated spectrum of the design for the analysis and design of the three intended structures. Specifications of the intended spectrum include BSE2 of ASCE / SEI41-06, modification factor of 8.0 (R = 8), and the additional coefficient of design regulations overstrength factor 2.0 ($\Omega_0 = 2$) is similar to the special eccentrically braced frame. The considered spectrum with the scale factor of $\frac{S_a \Omega_0}{R} g$ is applied to the structure for higher modes.

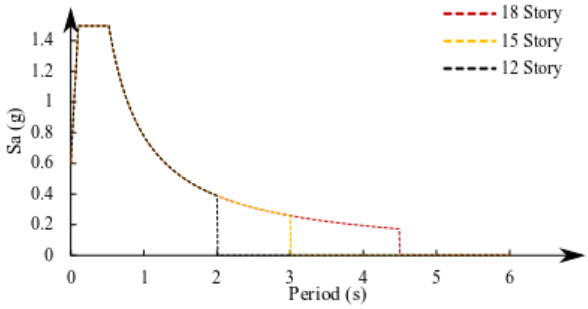

Fig. 11. Truncated design spectra

In the second software model, the frame is modeled with core sections designed under the forces of Set I and BRFs with reduced stiffness. Finally, by applying the forces of Sets I and II and the forces of the gravity system, the core sections of 12, 15, and 18-story structures are obtained according to **Table 2**.

377 **Table 2.** Member sections of the numerical model

Story Number	Story	Column	Brace	Beam	Tie
12-story	1	W 30 × 173	W 16 × 67	W 10 × 26	-
	2-3	W 30 × 173	W 16 × 67	W 10 × 26	W 30 × 108
	4-6	W 30 × 173	W 16 × 40	W 10 × 22	W 30 × 148
	7-9	W 30 × 148	W 16 × 40	W 10 × 22	W 30 × 132
	10-12	W 30 × 90	W 16 × 40	W 10 × 22	W 30 × 90
15-story	1	W 30 × 173	W 16 × 67	W 10 × 30	-
	2-3	W 30 × 173	W 16 × 67	W 10 × 30	W 30 × 173
	4-6	W 30 × 173	W16 × 31	W 10 × 22	W 30 × 132
	7-9	W 30 × 173	W 16 × 31	W 10 × 22	W 30 × 132
	10-12	W 30 × 148	W 16 × 31	W 10 × 22	W 30 × 132
	13-15	W 30 × 90	W 16 × 31	W 10 × 22	W 30 × 132
18-story	1	W 30 × 173	W 16 × 89	W 10 × 33	-
	2-3	W 30 × 173	W 16 × 26	W 10 × 22	W 30 × 148
	4-6	W 30 × 173	W 16 × 26	W 10 × 22	W 30 × 148
	7-9	W 30 × 173	W 16 × 26	W 10 × 22	W 30 × 148
	10-12	W 30 × 148	W 16 × 26	W 10 × 22	W 30 × 132
	13-15	W 30 × 108	W 16 × 26	W 10 × 22	W 30 × 108
	15-18	W 30 × 90	W 16 × 26	W 10 × 22	W 30 × 90

378

379 ## 3.2 Non-linear dynamic analyses

380 ### *3.2.1 Endurance Time Method analysis*

381 The scale coefficients obtained in this study are presented in **Table 3**. It should be noted that the
382 coefficients determined for earthquake records apply either the initial scale coefficients or the
383 Estekanchi coefficients. On the other hand, for ETAFs, the scale coefficient corresponding to each
384 level of risk can be determined with few trial-and-errors so that the corresponding previous section.
385 The example of scaled spectra of different ET ground motions at the MCE level for 15-story
386 BRDC-BRF is shown in **Fig. 12**.

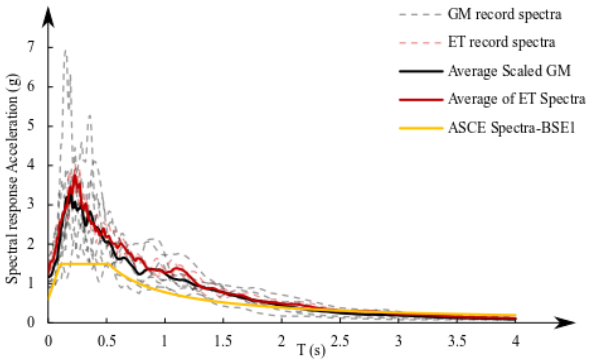

Fig. 12. MCE level design spectrum and 5% damped absolute acceleration spectra of the ground motion and ET records for 15-story BRDC-BRF.

Table 3. Scale factor and target time of proposed structures.

Story Number	Earthquake Hazard Level	Scale factor	ETA20en01 Target Time (s)	ETA20en02 Target Time (s)	ETA20en03 Target Time (s)	ET Scale factor
12-story	DBE	1.0258	10.0	10.0	10.0	1.02
	MCE	1.4304	15.0	15.0	15.0	1.02
15-story	DBE	1.1897	10.0	10.0	10.0	1.2
	MCE	1.6589	15.0	15.0	15.0	1.2
18-story	DBE	1.5787	10.0	10.0	10.0	1.65
	MCE	2.2014	15.0	15.0	15.0	1.65

As shown in **Fig. 13**, the BRF cross-sectional areas considered for the proposed structures are sufficient and can even be reduced to some extent. It is worth mentioning that the behavior of the structure at 15 seconds, which in the worst case is less than 2.5%. This result indicates the high ED of the structure. The maximum allowable values of the peak inter-story drifts for the two considered seismic hazard levels are summarized in **Table 4.** The permissible values are based on past research [28], and the following issues have been considered for their proper selection: 1) BRFs are yielded in 0.15% drift; Hence, the acceptable values have an appropriate distance from the beginning of fuses yielding. 2) Inter-story drift values always have higher values than Roof drift due to the effect of higher modes; therefore, the allowed values of roof drift are considered lower than inter-story drift to control inter-story value. Moreover, since the failure of BRFs occurs at 2.5% rad (inter-story drift), the permissible values are determined based on it.

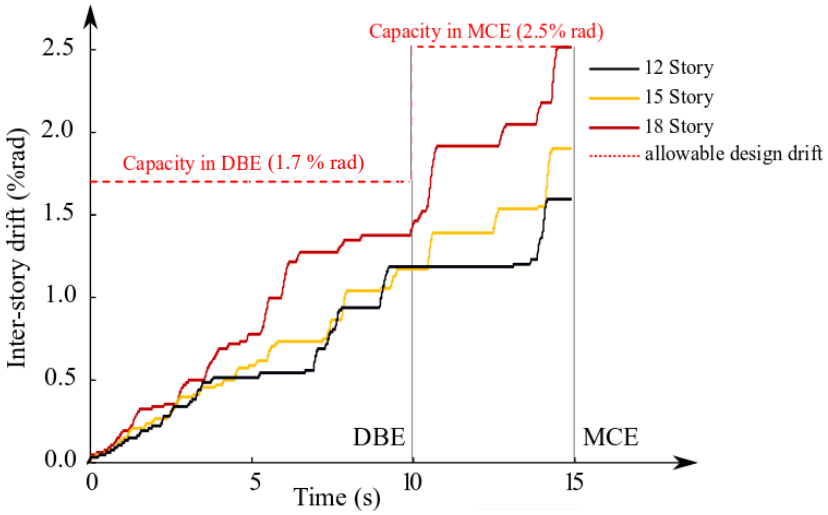

Fig. 13. Endurance time curve for 12, 15, and 18-story BRDC-BRF.

3.2.2 Peak roof drift and peak inter-story drift ratios

BRDC-BRF structures with GM set, and three ET records at DBE and MCE levels have been evaluated at this stage. **Fig. 14** shows the peak roof drift values at the two seismic levels of DBE and MCE. In the verification phase, the obtained peak values must be compared with the allowable/acceptable limits (roof and inter-story drift ratio) summarized in **Table 4**. The verifications are satisfied if the peak roof and inter-story drift (**Fig. 14**) values are less than allowable (**Table 4**).

Table 4. The performance level of structures studied for design.

Performance level	BRF yield	BRF yield	BRF failure
Hazard intensity	DBE	MCE	>MCE
Inter-story drift ratio	1.0 %-1.75%	1.75%-2.5%	>2.5%
Roof drift ratio	<1%	1.0%-1.5%	>1.5%

The average maximum roof drift of 12- 15- and 18-story structures are 0.76%, 0.87%, and 0.94% radian under GM set and 0.87%, 0.77%, and 0.74% radian under 3 ET records at the DBE level, respectively. Also, the maximum roof drift of 12- 15- and 18-story structures are 1.06%, 1.24%, and 1.25% radian under GM set and 1.12%, 1.11%, and 1.37% radian under 3 ET records at the

MCE level, respectively. So, the maximum roof drift at the DBE and MCE levels are less than 1.75% and 2.5%, respectively (allowable limit according to **Table 4**). If the mean maximum roof drift exceeds the allowable limit, the BRF area should be increased, and the BRDC-BRF structure should be redesigned. Furthermore, the ETAFs can estimate the maximum value of the roof drift at DBE and MCE levels. The maximum errors of the estimation of the ETAFs compared to conventional time history analysis are 21% and 10.2% at the DBE and MCE levels, respectively.

The inter-story drift is one of the essential response parameters to assess structural seismic vulnerability. So, this parameter for investigated structures is shown in **Figs. 15** and **16**. As can be seen, the mean inter-story drift at the DBE and MCE levels is slightly less than the allowable design drift (1.75% and 2.5%, respectively), according to **Table 4**.

The maximum inter-story drift of 12- 15- and 18-story structures are 1.05%, 1.23%, and 1.58% radian under GM set and 1.18%, 1.16%, and 1.39% radian under 3 ET records at the DBE level, respectively. Also, the maximum inter-story drift of 12- 15- and 18-story structures are 1.49%, 1.8%, and 2.14% radian under GM set and 1.58%, 1.88%, and 2.5% radian under 3 ET records at the MCE level, respectively. So, the maximum inter-story drift at the DBE and MCE levels are less than 1.75% and 2.5%, respectively (allowable limit according to **Table 4**). Furthermore, the ETAFs can estimate the maximum inter-story drift at DBE and MCE levels. Therefore, the maximum errors in estimating the ETAFs compared to conventional time history analysis are 12.3% and 16.9% at the DBE and MCE levels, respectively.

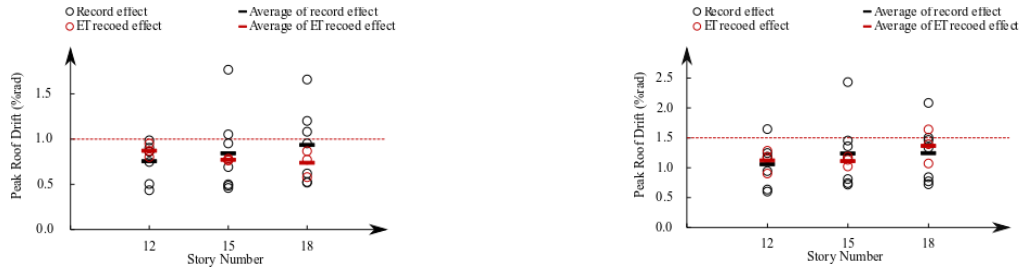

440 **Fig. 14.** Peak Roof drift; (a) DBE Level; (b) MCE Level.

441

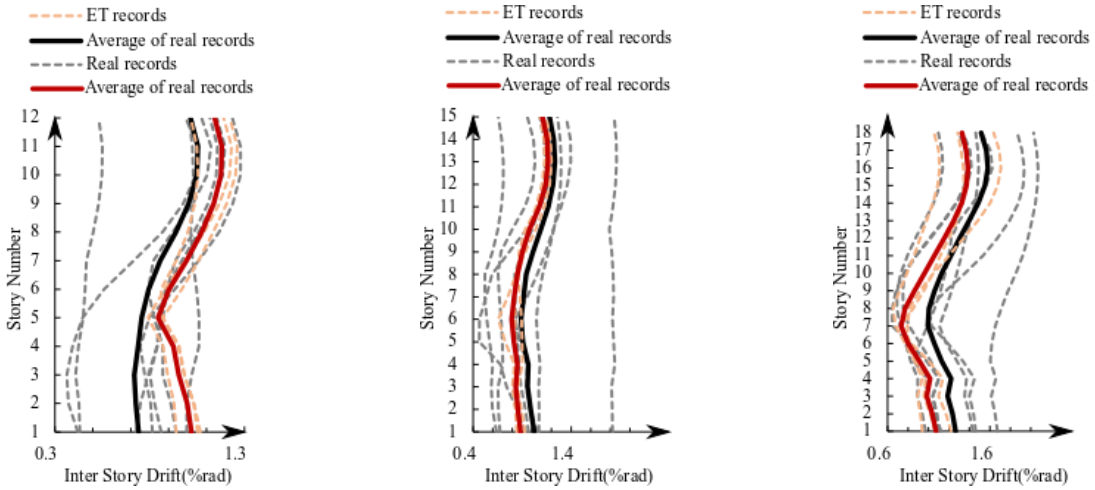

442 **Fig. 15.** Inter-story drift for DBE level; (a) 12 story; (b) 15 story; (c) 18 story.

443

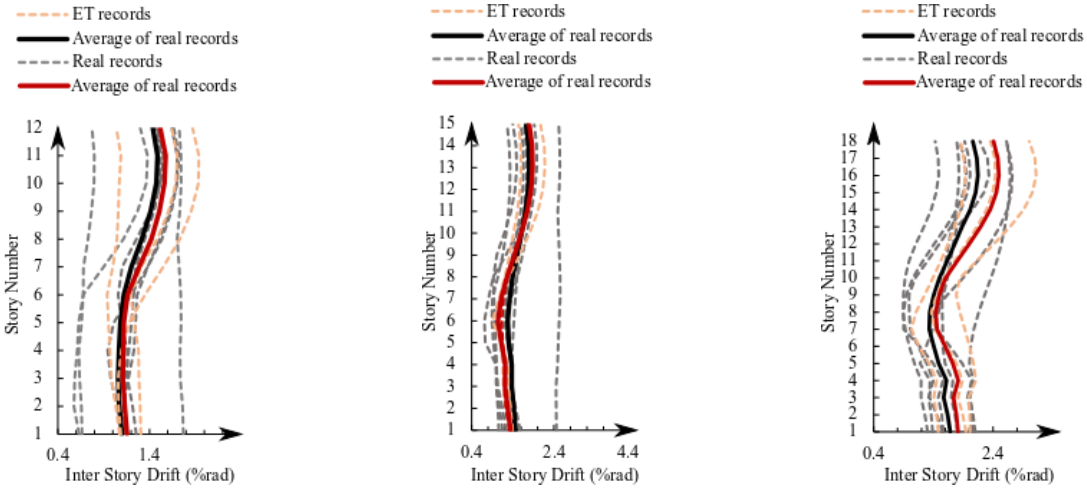

444 **Fig. 16.** Inter-story drift for MCE level; (a) 12 story; (b) 15 story; (c) 18 story.

445

3.2.3 *Deformation Concentration Factor*

The Deformation Concentration Factor, DCF, is an index that identifies the story drift concentration of BRDC-BRF systems; it determines the maximum story drift concerning the overall maximum roof drift and is calculated based on the following equation:

$$DCF = \frac{\max\left(\frac{d_i}{h_i}\right)}{\frac{\Delta r}{H}} \quad (3)$$

where d_i and h_i are the relative displacement and the height of the i^{th} floor, respectively. In addition, Δr and H are the maximum relative displacement and the structure's height, respectively. If DCF is equal to 1.0, it implies that the uniform inter-story drift distribution is achieved. Instead, if this value is higher than 1.0, drift concentration occurs in the structure and can lead to a soft-story mechanism. **Fig. 17** confirms that the BRDC-BRF structures at DBE and MCE levels have a DCF value less than 1.0 or very close to 1.0, indicating that these structures do not have soft-story failure and drift concentrations. The ETAFs can estimate the DCF index at the DBE and MCE levels. The determination errors of the ETAFs compared to conventional time-history analysis don't exceed 5.97% and 8.26% at the DBE and the MCE levels, respectively.

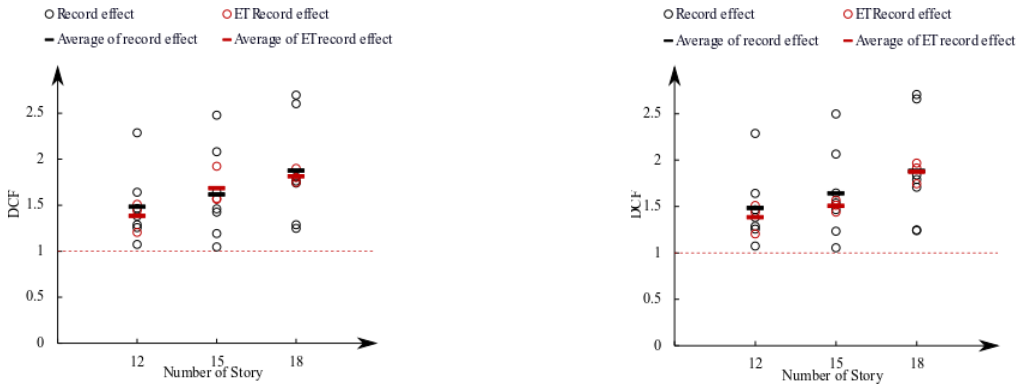

Fig. 17. DCF value; (a) DBE Level; (b) MCE Level.

3.2.4 Strength verifications of the structural members

Considering that the proposed method has been used to design the rocking cores, it is necessary to investigate the members' strengths, considering both axial strengths against tension and compression/buckling, bending, and shear. Thus, the maximum strains created in the farthest axis from the neutral axis of the sections have been investigated, and their value has been compared with the value of yield strains. **Fig. 18** shows the maximum strain of the columns sections, ties, beams, and braces in the two rocking cores at MCE seismic levels. According to these figures, in all elements of the earthquake level, the mean strain of the farthest section axis did not exceed the yield strain value, which confirms the accuracy of the proposed core method. Furthermore, the mean strain of the farthest section axis under endurance-time records results in a perfect estimate compared to other records.

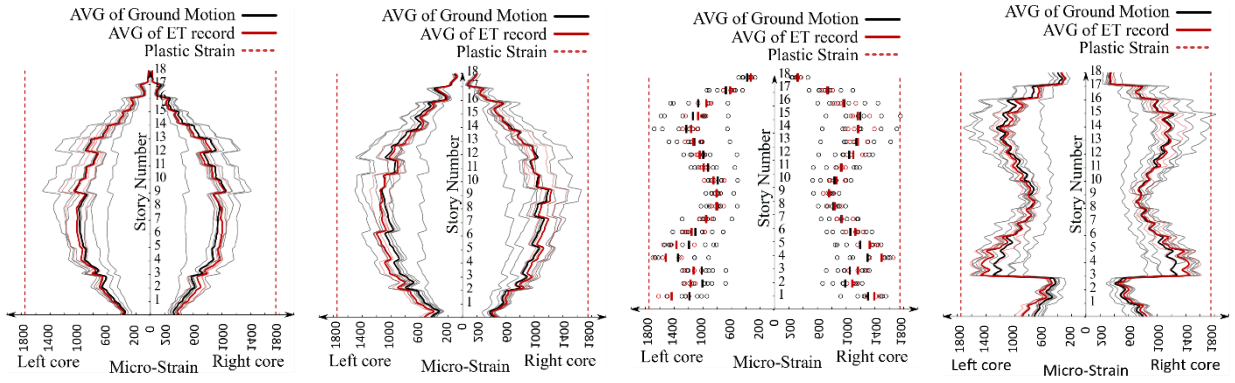

Fig. 18. The maximum strain in (a) columns, (b) ties, (c) beams, and (d) braces of the 9-story frame under MCE-level ground motions

4 Conclusions

This paper introduces a new type of rocking system called base-rocking dual-core braced-frame (BRDC-BRF) which results in limited column uplifting and high energy dissipating rate. In addition to providing an excellent structural response against severe earthquakes, this system also

prevents soft-story mechanisms. The proposed system is validated by means of an efficient design method which has been presented and corroborated by non-linear dynamic analysis.

In general, the results of this study are as follows:

- The analysis results of the time history of structures under GM set scaled at the DBE and MCE risk levels demonstrate the accuracy of the ET method. It was confirmed that in the optimal performance-based design of structures, which requires a frequent and large number of dynamic calculations and analyses, the ET method could predict the behavior of structures at different performance levels with a minimum number of analyses.
- The proposed design approach in this study considers two load sets. The first set examines the structure in the first mode corresponding to the maximum yielding capacity. If the capacity of sections or inter-story drift values does not meet the needs under dynamic loading, the design spectrum coefficient in the second load set (Set II, i.e., the force created by the higher modes) can be intensified.
- The roof drift is controlled by increasing the area of the BRF and the sections of the core members.
- One of the main features of the proposed system compared to the conventional systems is the easy interchangeability of the fuse elements (BRF elements) after a severe earthquake.
- Due to the high energy absorption of this system, smaller (hence cheaper) structural sections can be designed.
- The results show that the proposed system resolves both the problem of column uplifting and the high cross-section needed for post-tensioned cables as compared to other rocking systems.

Future studies in this area could be aimed at developing the fragility curves of the BRDC-BRF system. Furthermore, the seismic coefficients of BRDC-BRF systems should be determined for better and more practical seismic evaluation. Epistemic and aleatoric uncertainties always affect any numerical models [47]. Therefore, further investigation is needed to determine uncertainties such as frequent and non-frequent records used to evaluate the structural seismic performance [48], [49] and the uncertainties of elasticity modulus and yield strength of cores and fuses. Nonetheless, further investigations on the newly proposed BRDC-BRF system and ET method are encouraged through experimental tests.

References

[1] V. Broujerdian and E. Mohammadi Dehcheshmeh, "Locating the rocking section in self-centering bi-rocking walls to achieve the best seismic performance," *Bull. Earthq. Eng.*, 2022, doi: 10.1007/s10518-022-01325-y.

[2] M. R. Eatherton *et al.*, "Design concepts for controlled rocking of self-centering steel-braced frames," *J. Struct. Eng.*, vol. 140, no. 11, p. 4014082, 2014.

[3] Housner G, "The behavior of inverted pendulum structures during earthquakes," *pubs.geoscienceworld.org*, 1963.

[4] J. B. Mander and C.-T. Cheng, "Seismic resistance of bridge piers based on damage avoidance design," pp. 109–109, 1997.

[5] J. J. Ajrab, G. Pekcan, and J. B. Mander, "Rocking WallFrame Structures with Supplemental Tendon Systems," *J. Struct. Eng.*, vol. 130, no. 6, pp. 895–903, Jun. 2004, doi: 10.1061/(ASCE)0733-9445(2004)130:6(895).

[6] M. Pollino and M. Bruneau, "Seismic retrofit of bridge steel truss piers using a controlled rocking approach," *J. Bridg. Eng.*, vol. 12, no. 5, pp. 600–610, 2007.

[7] Y.-H. Chen, W.-H. Liao, C.-L. Lee, and Y.-P. Wang, "Seismic isolation of viaduct piers by means of a rocking mechanism," *Earthq. Eng. Struct. Dyn.*, vol. 35, no. 6, pp. 713–736, May 2006, doi: 10.1002/EQE.555.

[8] Y. Lu, "Inelastic behaviour of RC wall-frame with a rocking wall and its analysis incorporating 3-D effect," *Struct. Des. Tall Spec. Build.*, vol. 14, no. 1, pp. 15–35, Mar. 2005, doi: 10.1002/TAL.254.

[9] L. Chen, "Improving the Seismic Response of Tall Braced Streel Frames with Segmental Elastic Spine," Ecole Polytechnique de Montreal, 2018.

[10] F. C. Blebo, "Parametric Study of Seismic-Resistant Friction-Damped Braced Frame System.," University of Akron, Akron, OH., 2013.

[11] A. Kachooee, M. A. Kafi, and M. Gerami, "The Effect of Local Fuse on Behavior of Concentrically Braced Frame by a Numerical Study," *Civ. Eng. J.*, vol. 4, no. 3, p. 655, Apr. 2018, doi: 10.28991/cej-0309123.

[12] S. Ghasemi, M. F. Nezamabadi, A. S. Moghadam, and M. Hosseini, "Optimization of relative-span ratio in rocking steel braced dual-frames," *Bull. Earthq. Eng.*, vol. 19, no. 2, pp. 805–829, 2021, doi: 10.1007/s10518-020-00998-7.

[13] S. Moradi and H. V. Burton, "Response surface analysis and optimization of controlled rocking steel braced frames," *Bull. Earthq. Eng.*, vol. 16, no. 10, pp. 4861–4892, Oct. 2018, doi: 10.1007/s10518-018-0373-1.

[14] R. M. T. Takeuchi , X. Chen, "Seismic performance of controlled spine frames with energy-dissipating members," *J. Constr. Steel Res.*, 2015.

[15] F. C. Blebo and D. A. Roke, "Seismic-resistant self-centering rocking core system," *Eng. Struct.*, vol. 101, pp. 193–204, 2015, doi: 10.1016/j.engstruct.2015.07.016.

[16] M. Naghavi, R. Rahnavard, R. J. Thomas, and M. Malekinejad, "Numerical evaluation of the hysteretic behavior of concentrically braced frames and buckling restrained brace frame systems," *J. Build. Eng.*, vol. 22, pp. 415–428, Mar. 2019, doi: 10.1016/j.jobe.2018.12.023.

[17] "Midorikawa, M.; Azuhata, T.; Ishihara, T.; and Wada, A. (2006). 'Shaking Table Tests on Seismic Response of Steel Braced Frames with Column Uplift,' Earthquake Engineering and Structural Dynamics, 35(14), pp 1767-1785."

[18] "Tremblay, R., Poirier, L.-P., Bouaanani, N., Leclerc, M., Rene, V., Fronteddu, L., and Rivest, S. (2008). 'Innovative visously damped rocking braced steel frames.' Proc., 14th World Conf. on Earthquake Engineering, Beijing, China, October."

[19] "Lai, J. and Mahin, S. (2014). 'Strongback System: A Way to Reduce Damage Concentration in SteelBraced Frames.' J. Struct. Eng., 10.1061/ (ASCE) ST.1943-541X.0001198, 04014223."

[20] S. Hu, W. Wang, B. Qu, and M. S. Alam, "Development and validation test of a novel Self-centering Energy-absorbing Dual Rocking Core (SEDRC) system for seismic resilience," *Eng. Struct.*, vol. 211, May 2020, doi: 10.1016/j.engstruct.2020.110424.

[21] M. Palermo, V. Laghi, G. Gasparini, and T. Trombetti, "Coupled Response of Frame Structures Connected to a Strongback," *J. Struct. Eng.*, vol. 144, no. 9, p. 04018148, Jun. 2018, doi: 10.1061/(ASCE)ST.1943-541X.0002134.

[22] M. Bosco, E. M. Marino, and P. P. Rossi, "A design procedure for pin-supported rocking buckling-restrained braced frames," *Earthq. Eng. Struct. Dyn.*, vol. 47, no. 14, pp. 2840–2863, Nov. 2018, doi: 10.1002/EQE.3112.

[23] B. G. Simpson and S. A. Mahin, "Experimental and Numerical Investigation of Strongback Braced Frame System to Mitigate Weak Story Behavior," *J. Struct. Eng.*, vol. 144, no. 2, p. 04017211, Dec. 2017, doi: 10.1061/(ASCE)ST.1943-541X.0001960.

[24] M. S. Faramarzi and T. Taghikhany, "A comparative performance-based seismic assessment of strongback steel braced frames," *J. Build. Eng.*, vol. 44, p. 102983, Dec. 2021, doi: 10.1016/J.JOBE.2021.102983.

[25] P. Castaldo, B. Palazzo, F. P.-I. Sismica, and undefined 2016, "Fem simulations of a new hysteretic damper: The dissipative column," *Ing. Castaldo, B Palazzo, F PerriIngegneria Sismica, 2016•ingegneriasismica.org*.

[26] M. Palermo, V. Laghi, G. Gasparini, S. Silvestri, and T. Trombetti, "Seismic Design and Performances of Frame Structures Connected to a Strongback System and Equipped with Different Configurations of Supplemental Viscous Dampers," *Front. Built Environ.*, vol. 7, Oct. 2021, doi: 10.3389/FBUIL.2021.748087.

[27] L. Wiebe and C. Christopoulos, "Mitigation of higher mode effects in base-rocking systems by using multiple rocking sections," *J. Earthq. Eng.*, vol. 13, no. 1 SUPPL. 1, pp. 83–108, 2009, doi: 10.1080/13632460902813315.

[28] M. J. E. Majumerd, E. M. Dehcheshmeh, V. Broujerdian, and S. Moradi, "Self-centering rocking dual-core braced frames with buckling-restrained fuses," *J. Constr. Steel Res.*, vol. 194, p. 107322, 2022.

[29] M.J. Ebrahimi Majumerd, E. Mohammadi Dehcheshmaeh, and V. Broujerdian, "Feasibility study of using endurance time method for seismic evaluation of self-centering buckling restrained braced frame (SC-BRC-BF)," *Modares Civ. Eng. J.*, vol. 22, no. 2, p. 0, 2022.

[30] A. Whittaker *et al.*, "ATC-58 Project Task Report."

[31] E. Tafakori, S. Pourzeynali, and H. E. Estekanchi, "Probabilistic seismic loss estimation via endurance time method," *Earthq. Eng. Eng. Vib.*, vol. 16, no. 1, pp. 233–245, Jan. 2017, doi: 10.1007/s11803-017-0379-8.

[32] S. M. Razavi, "Investigation of Endurance Time in seismic analysis of steel frames as compared to Spectral Analysis Method," sharif university of technology, 2008.

[33] A. Bazmooneh and H. E. Estekanchi, "Determination of Target Time for Endurance Time method at Different Seismic hazard levels," *Sci. Iran.*, vol. 0, no. 0, pp. 0–0, Aug. 2017, doi: 10.24200/sci.2017.4176.

[34] L. Chen, R. Tremblay, and L. Tirca, "Practical seismic design procedure for steel braced frames with segmental elastic spines," *J. Constr. Steel Res.*, vol. 153, pp. 395–415, 2019, doi: 10.1016/J.JCSR.2018.10.010.

[35] S. Mazzoni, F. McKenna, M. H. Scott, and G. L. Fenves, "The Open System for earthquake engineering simulation (OpenSEES) user command-language manual," *Pacific Earthq. Eng. Res. Center, Berkeley, CA, USA*, 2009.

[36] M. A. Khaneghah, E. M. Dehcheshmaeh, V. Broujerdian, and G. G. Amiri, "Optimized design of dual steel moment resisting system equipped with cross-anchored self-centering buckling restrained chevron brace," *Earthquakes Struct.*, no. 23, p. 139, 2022.

[37] E. Mohammadi Dehcheshmeh and V. Broujerdian, "Determination of optimal behavior of self-centering multiple-rocking walls subjected to far-field and near-field ground motions," *J. Build. Eng.*, p. 103509, 2022, doi: https://doi.org/10.1016/j.jobe.2021.103509.

[38] E. Mohammadi Dehcheshmeh and V. Broujerdian, “Probabilistic Evaluation of Self-Centering Birocking Walls Subjected to Far-Field and Near-Field Ground Motions,” *J. Struct. Eng.*, vol. 148, no. 9, p. 4022134, 2022.

[39] M. H. Lavaei, E. M. Dehcheshmeh, P. Safari, V. Broujerdian, and A. H. Gandomi, “Reliability-based design optimization of post-tensioned self-centering rocking steel frame structures,” *J. Build. Eng.*, p. 106955, 2023.

[40] ASCE, *Minimum Design Loads for Buildings and Other Structures, ASCE/SEI 7-10,*. American Society of Civil Engineers (ASCE), Reston, VA., 2010.

[41] O. Ghashang pour peivasty, “Experimental Study of Buckling Restrained Brace (BRB),” University of Tabriz, 2016.

[42] ASCE, *Seismic Rehabilitation of Existing Buildings, ASCE/SEI 41-06,*. American Society of Civil Engineers (ASCE), Reston, VA., 2007.

[43] “FEMA-440.: Improvement of Nonlinear Static Seismic Analysis Procedures. Federal Emergency Management Agency (2005).”

[44] A. Farhadi, “Seismic Performance Evaluation of Steel Frame With Tuned Mass Damper Using Endurance Time Method,” sharif university of technology, 2010.

[45] H. E. Estekanchi, V. Valamanesh, and A. Vafai, “Application of Endurance Time method in linear seismic analysis,” *Eng. Struct.*, vol. 29, no. 10, pp. 2551–2562, Oct. 2007, doi: 10.1016/J.ENGSTRUCT.2007.01.009.

[46] H. Estekanchi, A. VAFAEI, and A. SADEGH, “Endurance time method for seismic analysis and design of structures,” 2004.

[47] P. Castaldo, G. Amendola, L. Giordano, and E. Miceli, “Seismic reliability assessment of isolated multi-span continuous deck bridges,” *Ing. Sismica*, vol. 39, no. 3, 2022.

[48] S. Kitayama and M. C. Constantinou, “Collapse performance of seismically isolated buildings designed by the procedures of ASCE/SEI 7,” *Eng. Struct.*, vol. 164, pp. 243–258, Jun. 2018, doi: 10.1016/J.ENGSTRUCT.2018.03.008.

[49] G. Auad, P. Castaldo, and J. L. Almazán, “Seismic reliability of structures equipped with LIR-DCFP bearings in terms of superstructure ductility and isolator displacement,” *Earthq. Eng. Struct. Dyn.*, vol. 51, no. 13, pp. 3171–3214, Oct. 2022, doi: 10.1002/EQE.3719.

Appendix 1

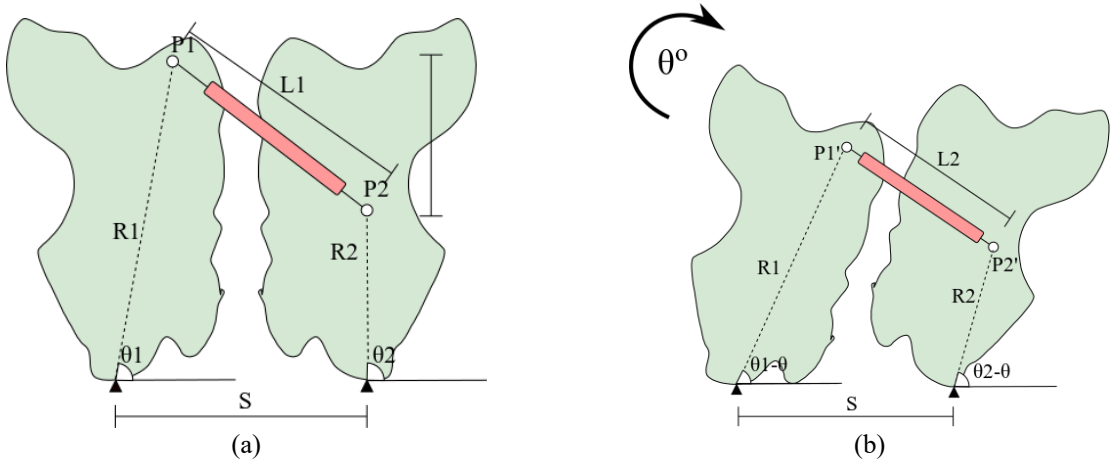

Fig. a1. (a) Initial position; (b) rotation position

By assuming the initial length of the BRF is equal to L_1, the secondary length of the BRF is calculated by changing the length of Δ as follows;

$$L_2 = L_1 + \Delta \xrightarrow{L_2^2} L_2^2 - L_1^2 = \Delta^2 + 2\,\Delta\,L_1 \xrightarrow{*(1/L_1^2),\ \Delta/L1=\zeta} (L_2^2 - L_1^2)/\,L_1^2 = \zeta^2 + 2\,\zeta \xrightarrow{\zeta^2 \sim 0} \zeta = (L_2^2 - L_1^2)/\,2L_1^2 \rightarrow \zeta \propto (L_2^2 - L_1^2) \quad \text{(a1)}$$

In the above equation, ζ is the axial strain of BRF. The coordinates of the beginning and end points of the BRF in the initial state are as follows;

$$P_1 \text{ coordinate: } P_{1x} = R_1 \cos(\theta_1),\ P_{1y} = R_1 \sin(\theta_1)$$
$$P_2 \text{ coordinate: } P_{2x} = S + R_2 \cos(\theta_2),\ P_{2y} = R_2 \sin(\theta_2) \quad \text{(a2)}$$

In the above equation, S is the distance between the point of rotation of the two cores at the base, and the coordinates of the beginning and end points of the BRF in the second state (core rotation as θ), assuming $\sin(\theta/2) \sim \theta/2$ are as follows;

$$P_1' \text{ coordinate: } P_{1x}' = R_1 \cos(\theta_1) + R_1\,\theta \cos(90\text{-}\theta_1\text{+}\theta/2),\ P_{1y}' = R_1 \sin(\theta_1) + R_1\,\theta \sin(90\text{-}\theta_1\text{+}\theta/2)$$
$$P_2' \text{ coordinate: } P_{2x}' = S + R_2 \cos(\theta_2) + R_2\,\theta \cos(90\text{-}\theta_2\text{+}\theta/2),\ P_{2y}' = R_2 \sin(\theta_2) + R_2\,\theta \sin(90\text{-}\theta_2\text{+}\theta/2) \quad \text{(a3)}$$

Assuming $\theta^2 \sim 0$ and $\cos(\theta_1 - \theta/2) \sim \cos(\theta_1)$, the value $(L_2^2 - L_1^2)$ considering $L^2 = \Delta P_x^{\,2} + \Delta P_y^{\,2}$ and simplification is calculated as follows;

$$L_2^2 - L_1^2 = 2S\theta R_1 \sin(\theta_1) - 2S\theta R_2 \sin(\theta_2) \quad \text{(a4)}$$

By placing the above relation in **Equation a1**, we have;

$$\zeta \propto 2S\theta(R_1 \sin(\theta_1) - R_2 \sin(\theta_2)) = 2S\theta\Delta h \quad \rightarrow \quad \zeta \propto S\,\Delta h\,\theta \tag{a5}$$

In the above relations, the parameters of R1, R2, θ1, θ2, and Δh are shown in **Fig. a1**. According to **Equation a5**, the amount of axial strain created by BRF is directly related to the three parameters of S, Δh, and θ. The θ parameter depends on the lateral force, the S parameter depends on the distance between the core supports, and the Δh parameter depends on the vertical height of the two ends of the BRF. Assuming its constant length in the vertical state of BRF, its maximum strain value is obtained.